Iranian Journal of Hydrogen & Fuel Cell 2(2021) 113-125

Iranian Journal of Hydrogen & Fuel Cell

IJHFC

Journal homepage://ijhfc.irost.ir

Numerical Investigation of a Hydrogen-fuelled Planar AP-SOFC Performance with Special Focus on Safe Operation

Majid Kamvar[a,*] and Robert Steinberger-Wilckens[b]

[a]Assistant Professor, Department of Mechanical Engineering, Parand Branch, Islamic Azad University, Parand, Iran
[b]Professor, Center for Fuel Cell and Hydrogen Research, School of Chemical Engineering, University of Birmingham, Edgbaston, B15 2TT, UK

Article Information

Article History:

Received:
06 Sep 2021
Received in revised form:
14 Nov 2021
Accepted:
18 Nov 2021

Keywords

All porous
Solid oxide fuel cell
Hydrogen-fuelled
Safe operation
Porous electrolyte

Abstract

The All-Porous Solid Oxide Fuel Cell (AP-SOFC) is a scheme that links a dual and single chamber SOFC, combining the potential advantages of both. The AP-SOFC is a novel concept that benefits from dual-chamber SOFC technology with a porous electrolyte, which allows the tunned distribution of oxygen on the anode side that allows the controlling of air and fuel distribution that is not possible in a single chamber scheme of SOFC.

Intermixing of fuel and air in AP-SOFC systems could cause the formation of explosive gas mixtures, especially when hydrogen is used as fuel due to its high flammability in air mixture. Thus, the aim of this study is to investigate the safe operation of a hydrogen-fuelled planar AP-SOFC using a two-dimensional finite element method based numerical model. To achieve this goal, different combinations of the hydrogen and oxygen inlet mole fraction are considered. Since a change in the inlet mole fraction of hydrogen and oxygen can affect the cell performance, four safe conditions for these combinations are chosen and compared. Finally, the best combination of the inlet mole fraction of hydrogen and oxygen having both safe operation and enhanced cell performance is reported.

1. Introduction

Burning fossil fuels to achieve energy supplies harms our environment by increasing greenhouse gas concentration in the Earth's atmosphere [1]. Fuel cells as an eco-friendly technology for providing electricity and heat could be a suitable alternative to conventional sources of energy [2]. Fuel cells convert the chemical energy available in chemical species directly to

*Corresponding author. mkamvar@mail.kntu.ac.ir
Tel: +9821-5673-3037

doi: 10.22104/IJHFC.2021.5181.1229

electrical energy by electrochemical reactions without any combustive conversions [3]. Fuel cells are divided into different categories based on their electrolyte material.

Solid Oxide Fuel Cells (SOFCs) in which a solid ceramic is used as the electrolyte layer operate at higher temperatures (above 500°C) between different types of fuel cells [4]. This higher range of operating temperature has some advantages, including high efficiency in energy conversion and the ability to use a variety of fuels [5]. However, SOFCs, especially in a stack design, suffer from sealing problems at this high range of temperatures [6]. As an alternative for achieving the enhanced reliability and shock-resistant of SOFC, Hibino and Iwahara introduced the sealing-free structure of single chamber solid oxide fuel cells (SC-SOFCs) in 1993 [7]. In SC-SOFCs, both the anode and the cathode are exposed in the same gas chamber resulting in a more compact and simplified stack design [8]. However, the performance of SC-SOFCs compared to conventional SOFCs is quite low [9, 10]. This is due to the intermixing of the fuel and the oxidant before insertion into the cell layers, which leads to an increase in the concentration overpotential of the cell.

Some efforts have been made to enhance the low performance of the SC-SOFC. Tian et al. enhanced the performance of a single chamber solid oxide fuel cell by using a dual gas supply [11]. They claimed that using a dual gas supply method increased the maximum power density by 67%. Bedon et al. [12] introduced a specific material for the cathodes of SC-SOFC. They successfully fabricated and tested CFA and CFA + FeO_x cathode material to obtain a material with specific properties in terms of process efficiency. Akhtar et al. [13] analyzed the hydrodynamic/electrochemical performance of an SC-SOFC operating on a nitrogen diluted hydrogen/oxygen mixture using a three-dimensional numerical model based on the finite element method. They included safety issues in their study as well. The same authors also successfully fabricated and tested an anode-supported, micro-tubular solid oxide fuel cell operated under single chamber conditions [14]. Their cell showed 1.05 V maximum open-circuit voltage (OCV) and a maximum power output of 122 mW cm^{-2} at a methane/air ratio of 1:4.76 and 750°C operating temperature. Building on their past work, they then developed the three single-cells, arranged in a triangular configuration, of the SC-SOFC stack [15].

Akhtar et al. advanced their research on enhancing the SC-SOFC performance with the aid of numerical tools as well [16-19]. Kamvar et al. worked on enhancing the performance of the SC-SOFCs numerically, too [9-10, 20]. Although these studies present some potential advantages of SC-SOFCs, the lack of simultaneous access to high power density and high fuel efficiency remains an obstacle to its commercialization [10]. To overcome this problem, a novel concept of dual chamber SOFC technology, entitled the all-porous solid oxide fuel cell (AP-SOFC), was designed and introduced by Gue et al. in 2013 [21]. In this scheme, the electrolyte layer structure (similar to the other two electrode layers) is porous, which allows the intermixing of air and fuel to occur inside the cell. In other research, Gue et al. [22] studied the effect of support types on the AP-SOFC performance under coke-free and lack of flammability probability conditions. They reported that the performance of the anode-supported cell was over 14 times more compared to the electrolyte-supported one. However, the number of studies conducted in the area of AP-SOFC is very low. To our knowledge, apart from Gue et al.'s studies, only Xu et al. have worked numerically on the performance of the methane-fuelled AP-SOFC scheme as an extension of Gue et al.'s studies [23-25].

All these research works have been limited to AP-SOFC using methane as fuel in order to prevent coke formation at the anode , the main problem of methane-fuelled SOFC reliability. Using hydrogen as a fuel has some advantages. It is environmentally benign, produces high energy density per weight and low en-

ergy density per volume with proper storage, and has a synergistic effect with current industrial waste heat [26]. Kamvar [27], in his very recent study, presented a comparative study examining the effects of the flow configuration of a planar hydrogen-fuelled AP-SOFC on cell performance. His results showed that the counter flow configuration concept reveals better cell performance. However, safety issues were not involved in this study.

The aim of this study is to present a numerical model of a planar AP-SOFC using hydrogen fuel considering the safe operation. Since the flammability of hydrogen in the air is high, the safe operation needs to be carefully designed. Thus, the chief purpose of this paper is to present a parametric study in order to define operating conditions that not only keep the system safe but also maintain the cell performance as high as possible.

2. Problem Definition

The previously validated model from [27] is used and extended to include the safe operation of the cell. All governing equations and cell structures are the same. Thus, the readers are referred to [27] for more information. Fig. 1 shows the schematical geometry of the problem. As shown in the figure, the porous structure of the electrolyte layer in AP-SOFCs enables the fuel and air to be intermixed. The high flammability of hydrogen in an oxidant atmosphere is a risk for system safety of hydrogen-fuelled AP-SOFCs. Numerical tools help to evaluate this issue before performing tests in the laboratory. Assuming the electrodes to be selective, the following electrochemical reactions occur in the anode and cathode electrodes, respectively:

$$H_2 + O^{-2} \rightarrow H_2O + 2e^- \quad (1)$$

$$O_2 + 2e^- \rightarrow O^{-2} \quad (2)$$

All geometrical, micro-structural, and thermophysical parameters of the modelled cell follow the experimental base case reported by Timurkutluk et al. [28] in order to present more realistic cell behaviour.

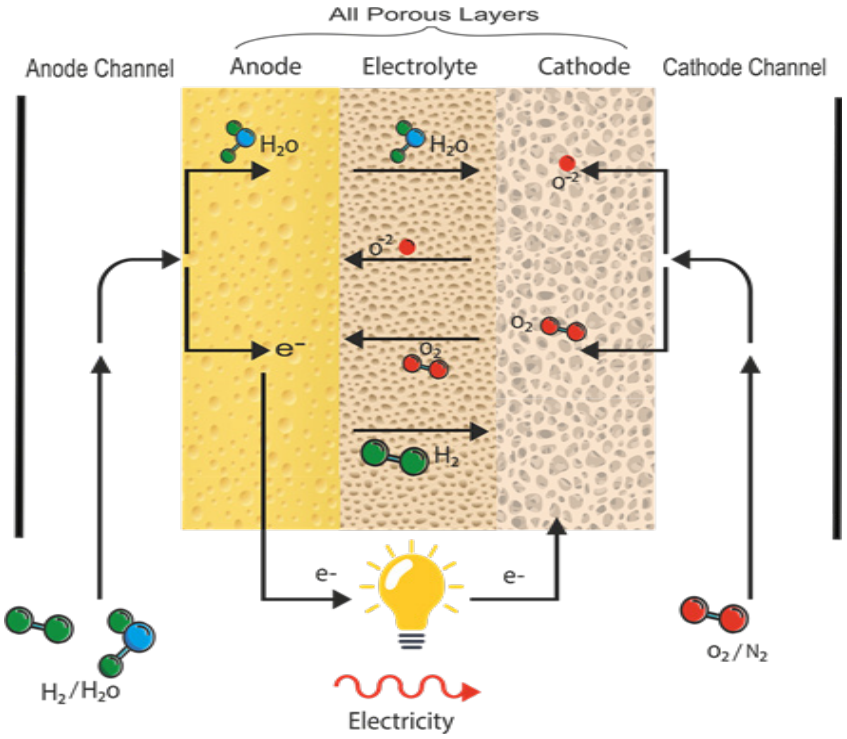

Fig. 1. Schematic view of problem.

To avoid verbosity, all physical equations governing this problem were based on the previous study's assumptions [27], and are described briefly in this section:

- The steady-state form of continuity equation [29]:

$$\nabla.(\rho u) = 0 \quad (3)$$

where ρ is the density of the mixture and is calculated by the ideal gas equation and **u** is the velocity vector. Fluid flow equation in free-media of channels [30]:

$$\rho(u.\nabla)u = \nabla.(-pI + \mu(\nabla u + (\nabla u)^T) - 2\mu(\nabla u)I) \quad (4)$$

- Fluid flow equation in porous-media of cell layers by neglecting inertial term [29]:

$$\frac{\rho}{\varepsilon}\left((u.\nabla)\frac{u}{\varepsilon}\right) = \nabla.\left(-pI + \frac{\mu}{\varepsilon}(\nabla u + (\nabla u)^T) - \frac{2\mu}{3\varepsilon}(\nabla u)I\right) \quad (5)$$

- Multicomponent diffusion equation of gaseous species [31]:

$$\nabla.j_i + \rho(u.\nabla)\omega_i = R_i \quad (6)$$

Where R_i is the source term that accounts for mass deposit or mass creation of the *i*th species due to electrochemical reactions and is formulated as [13]:

$$R_{H_2} = -\frac{j_{v,a}}{2F} \quad (7)$$

$$R_{H_2O} = \frac{j_{v,a}}{2F} \quad (8)$$

$$R_{O_2} = -\frac{j_{v,c}}{4F} \quad (9)$$

Where j_v is the local current source within electrode functional layers per unit volume obtained by the Butler-Volmer equation [27] and F is Faraday's constant (equal to 96487 C/mol).

The Energy equation including convection and conduction terms [32]:

$$\nabla.(\rho C_p u T - k\nabla T) = Q \quad (10)$$

Where C_p is the specific heat, k is the thermal conductivity, and Q is the energy source term due to ionic transport resistance ($Q_{ohm,io}$), reversible (Q_{rev}) and irreversible (Q_{irr}) heat generations, which are formulated respectively in Eqs. (11) to (13) [3]:

$$Q_{omh,io} = \sigma_i \nabla\phi_i.\nabla\phi_i \quad (11)$$

Where, σ_i is the ion conductivity and ϕ_i is the ion potential.

$$Q_{rev} = T\,\Delta s\,(\frac{i}{zF}) \quad (12)$$

Where Δs is the entropy change of the H_2-oxidation half-reaction at the anode electrode or the O_2-reduction half-reaction at the cathode electrode, T is the absolute temperature, i is the current density, z is the number of electrons participating in electrochemical reactions, and F is the Faraday's constant

$$Q_{irr} = \eta_{act}.i_v \quad (13)$$

Where η_{act} is the activation overpotential, and the

current density for the electrode side, i_v, is calculated by the Bulter-Volmer's equation.

- Electronic and ionic current distribution equations [3]:

$$-\nabla.(\sigma_e \nabla \phi_e) = i_{v,e} \quad (14)$$

$$-\nabla.(\sigma_i \nabla \phi_i) = i_{v,i} \quad (15)$$

Where $i_{v,e}$ and $i_{v,i}$ are the electronic and ionic source terms obtained by Butler-Volmer's equation. Note that these terms are valid in the functional layers where conduct current is in both an electrolyte and an electrode phase.

It was necessary to understand the boundary conditions for each physics to fulfill the mathematical modeling. The conditions applied to the boundaries of the current geometry of the problem are fully described in [27].

3. Numerical procedure

The problem equations were solved using COMSOL Multiphysics 5.2a with the aid of the Finite Element Method (FEM). The mesh consisted of 10606 triangular elements of good quality in which more refined elements were considered in functional layers where a higher resolution was necessary. To control the solution procedure, the set of equations were solved in steps. The total computing time for all steps was about 22 min.

4. Results and discussion

4.1. A comparative study

In this section, a comparative study between a conventional (two chamber) SOFC and an AP-SOFC will be investigated. The previously validated model [27] is used in this study. To have a more realistic comparison, all input parameters given in [27] are maintained. Fig. 2 depicts the comparative performance between a conventional planar SOFC and an AP-SOFC with 30% electrolyte porosity, with the same input parameters given in [27] for an operating temperature of 750°C. It is clear that the conventional SOFC shows a better performance than the AP-SOFC, as expected according to the relatively lower partial pressures of reactants and their mixing. The maximum power density produced by the sample conventional SOFC is about 3596 W/m^2, while the value for the AP-SOFC is 2540 W/m^2, showing a 29% decline in maximum power density produced by the cell. Two key factors play a major role in this low AP-SOFC performance: i) the porous electrolyte, as compared to a dense one, displays a lower ionic conductivity because oxide ions are able to diffuse only through the solid portion of the electrolyte, and ii) the diffusion and transportation of inactive species via the porous electrolyte from anode to cathode and vice versa reduces the cell performance.

Fig. 3 depicts the x component of the total flux of hydrogen, oxygen, and water species through the anode-electrolyte interface at 0.7V cell voltage and 750°C operating temperature. Note that the x component of the total flux of oxygen is negative, indicating that oxygen diffuses from the cathode side to the anode side (the opposite direction of the x-axis) while this value is positive for hydrogen and water species as these species diffuse from the anode to the cathode side. For better comparison, the total flux of the oxygen values is multiplied by -1, as shown in Fig. 3. It is found that the total flux of water compared to the other two species is quite low, while oxygen has the highest value. The amount of oxygen total flux reveals a jump from 16 g.m^{-2}.s^{-1} to 27.7 g.m^{-2}.s^{-1} around y=0 mm, then it descends to about zero. A slight backflow of oxygen from the anode to the cathode side is observed

around the outlet. The hydrogen total flux distribution shows different behaviour, dropping from 14 $g.m^{-2}.s^{-1}$ to 3.75 $g.m^{-2}.s^{-1}$ around the inlet, then changing slightly to 1.75 $g.m^{-2}.s^{-1}$. It is concluded that the mass flow of species in the zone close to the inlet is high, which should be taken into account in the analysis of system safety issues.

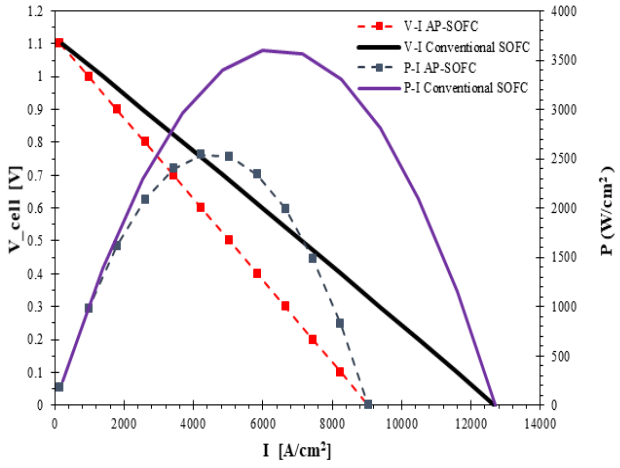

Fig. 2. A comparative performance representation of a conventional SOFC and an AP-SOFC with 30% electrolyte porosity, calculated with the same input parameters.

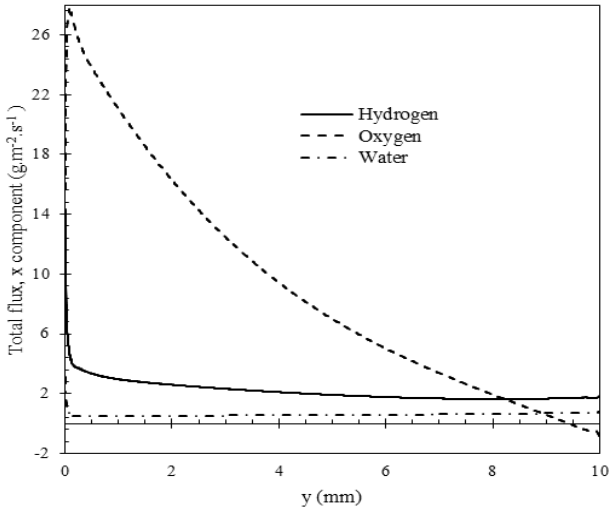

Fig. 3. The x component of the total flux of hydrogen, oxygen, and water species at cell voltage 0.7V along with the anode-electrolyte intersection at 750oC operating temperature. For better comparison, the flux of oxygen has been inverted; therefore, a high positive flux is from the cathode to anode, whereas it is from anode to cathode for both hydrogen and water.

Figs. 4 (a)-(f) show different species molar concentration distributions along the y-axis (see Fig. 1) crossing the middle of the electrode channel as well as the electrode functional layer at cell voltage 0.7 V and 750°C operating temperature. It is obvious from Figs. 4a and 4b that hydrogen is consumed on the anode side; however, the hydrogen depletion within the AP-SOFC is noticeably more rapid compared to the conventional SOFC. Hydrogen in the anode channel and anode functional layer of the conventional SOFC is reduced by 2.2% and 2.38%, respectively, while these values are 37.4% and 30.2%, respectively, for the AP-SOFC. This shows that the depletion of fuel in the AP-SOFC compared to the conventional SOFC, especially in its anode channel, is noticeably higher. Also, the rate of hydrogen reduction in both the anode channel and functional layer of the conventional SOFC, unlike the AP-SOFC, is almost the same. However, the hydrogen amount in both the conventional SOFC and AP-SOFC decreases along the direction of flow. Water in the conventional SOFC and AP-SOFC shows two different behaviours. According to Figs. 4c and 4d, the water amount in the anode channel and anode functional layer of the conventional SOFC increased by 28.3% and 32.1%, respectively, while the water amount in the anode channel of the AP-SOFC is reduced by 17.2%. In the anode functional layer of the AP-SOFC, the water amount dropped from 0.275 mol/m^3 to 0.224 mol/m^3 at about y=0.3mm, and after this, it increased slightly to 0.2655 mol/m^3. As shown in Figs. 4e and 4f, the oxygen amount within the cathode channel and cathode functional layer of the conventional SOFC decreased by only 2.76% and 3.31%, respectively. While the reduction in the oxygen amount within the cathode channel and cathode functional layer is noticeably higher compared to the conventional SOFC, it was reduced by 48.87% and 22.1% within the cathode channel and cathode functional layer, respectively.

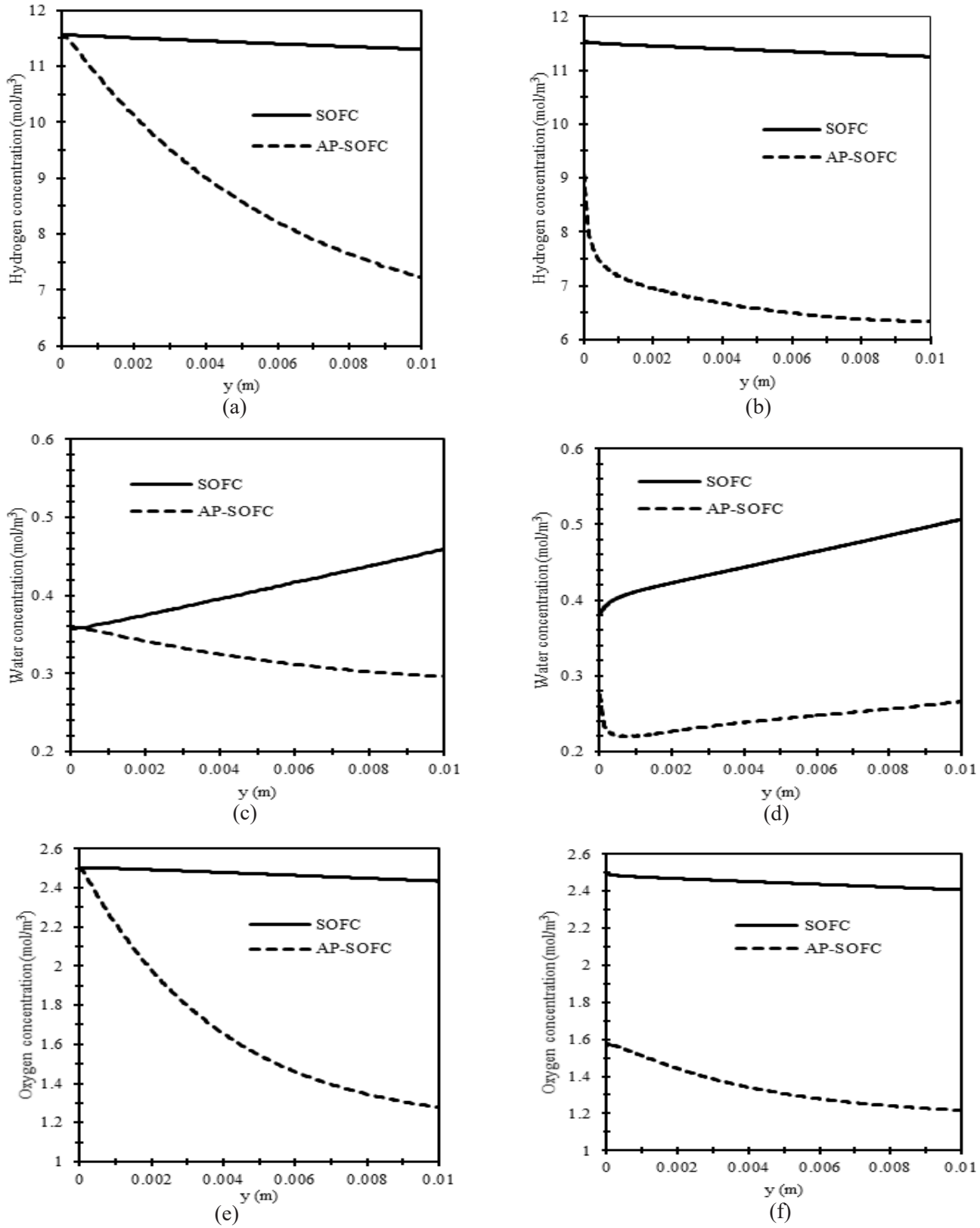

Fig. 4. A comparison of the molar concentration of different species within a conventional SOFC and an AP-SOFC, respectively, along the y axis: (a) and (b) are the hydrogen molar concentration distribution along the middle of the anode channel and anode functional layer, respectively, and (c) and (d) are the water molar concentration distribution along the middle of the anode channel and anode functional layer, respectively. (e) and (f) show the oxygen molar concentration distribution along the middle of the cathode channel and cathode functional layer, respectively. All figures are at a 750oC operating temperature and a cell voltage of 0.7V.

Fig. 5 shows the cell voltage versus maximum cell temperature occurring within the cell for both SOFC and AP-SOFC schemes. It is clear that the maximum cell temperature increases with decreasing cell voltage since decreasing electrical efficiency brings a higher heat production. However, it is understood from the figure that the conventional SOFC reveals higher maximum temperature compared to the AP-SOFC scheme since the current at a given current density will be higher, thereby increasing the Ohmic heat produced.

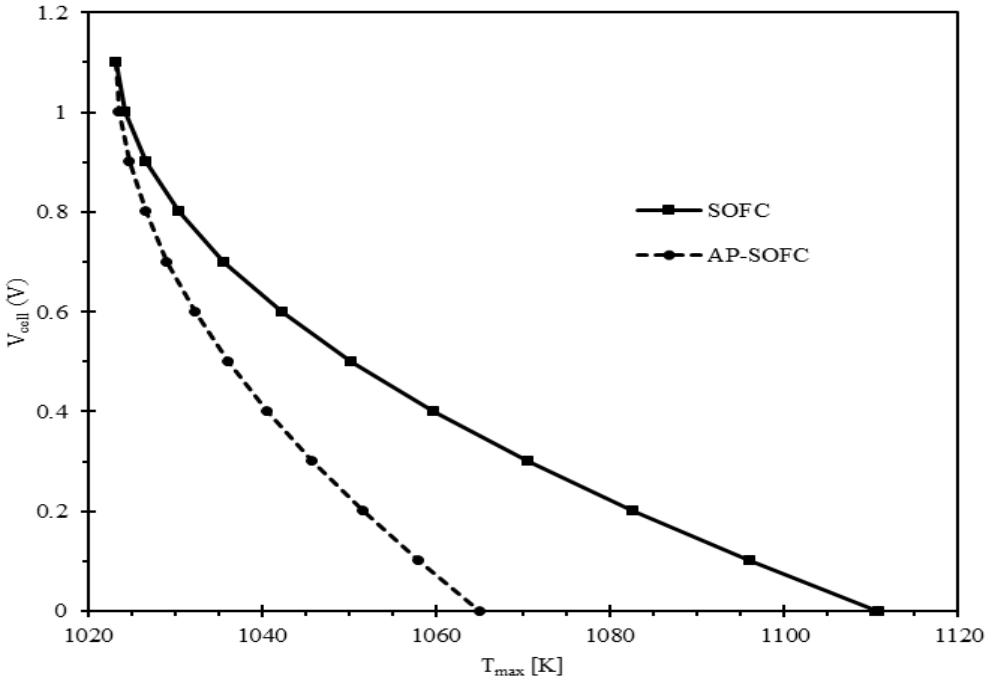

Fig. 5. The cell voltage versus maximum cell temperature occurring within the cell for both SOFC and AP-SOFC schemes at 750oC operating temperature.

4.2. Safe operation issue

As stated before, the flammability of hydrogen in oxygen is extremely high in the operating temperature range. To evaluate the risk of hydrogen combustion or explosion, the concentration of hydrogen is suggested to be lower than the Lower Explosive Limit, which is 4% in the air (21% oxygen). Thus, the mole fraction of $H_2 \times O_2$ should be equal to or less than 0.84% for the safe operation of the current AP-SOFC design. The distribution of the $H_2 \times O_2$ mole fraction product is shown in Fig. 6. As shown in Fig. 6b, only a small zone near the inlet (grey zone) is safe, and the part of the cell that is exposed to flammable hydrogen mixtures should be controlled; although, the risk of flammable hydrogen mixtures forming in the anode electrode is more probable.

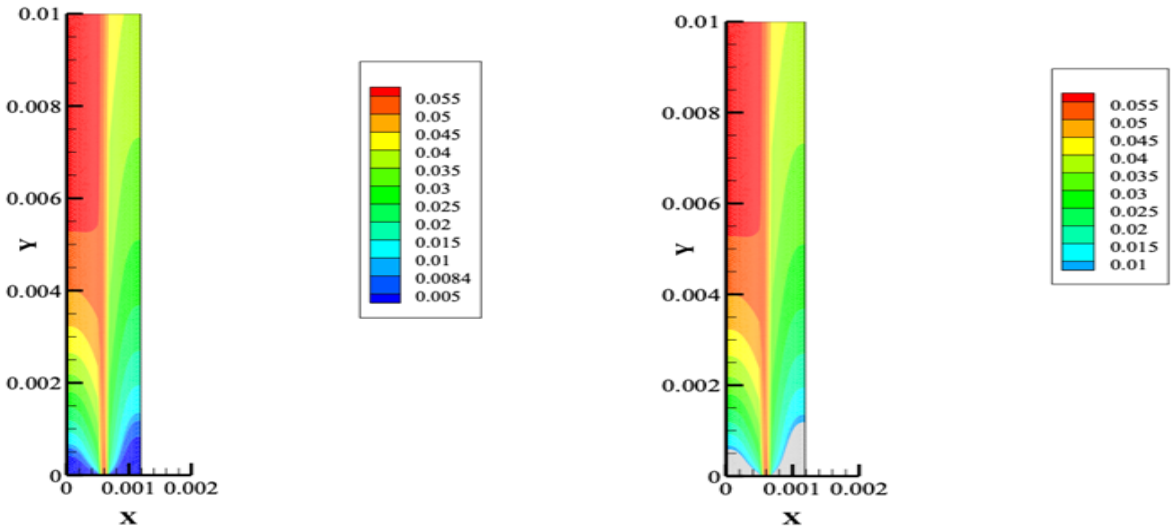

Fig. 6. a) H2×O2 mole fraction product at cell voltage 0.7V for a 30% electrolyte porosity AP-SOFC with a 0.97 and 0.4 H2/O2 inlet mole fraction, respectively. b) Cut-off H2×O2 mole fraction product below 0.84%.

In order to control the safe operation of the current AP-SOFC, two determining factors are examined: i) the hydrogen inlet mole fraction and ii) the oxygen inlet mole fraction. It is expected that decreasing hydrogen and oxygen inlet mole fractions will improve cell safety operation. However, decreasing the H_2/O_2 inlet mole fractions reduced the cell performance by reducing the open circuit voltage. Thus, it is important to achieve a balance between safe operation and enhanced performance of the cell. Fig. 8 shows the $H_2 \times O_2$ mole fraction product at cell voltage 0.7V in a 30% electrolyte porosity AP-SOFC for different combinations of H_2 and O_2 inlet mole fractions. As shown in Fig. 7, the safe region of the cell (grey region) is extended by decreasing H_2 and O_2 inlet mole fractions until, in cases 5 and 6, safe operation is achieved. It can be also seen in Fig. 7 that the electrolyte layer near the inlet is more exposed to risk, and this region is the last to become safe. To present a more comprehensive analysis based on the safety issue, the maximum value of the mole fraction of $H_2 \times O_2$ is considered the checkpoint, and all combinations of H_2/O_2 inlet mole fractions result in a mole fraction of $H_2 \times O_2$ less than 0.84% at cell voltage 0.7V are selected and plotted in Fig. 8. Note that the limiting line separating the safe combinations of H_2/O_2 inlet mole fractions is approximated by a 4th order polynomial using curve-fitting:

$$x_{H_2,in} \le 435.58529x_{o_2,in}^4 - 382.21241x_{o_2,in}^3 + 125.179375x_{o_2,in}^2 - 18.917046x_{o_2,in} + 1.29856494 \quad (27)$$

A comparison study was used to extract the best combination of hydrogen and oxygen inlet molar fractions, meeting both best cell performance and safe operating conditions. Four cases of 0.5/0.06, 0.6/0.05, 0.7/0.04 and 0.96/0.02 of H_2/O_2 for inlet mole fractions were considered. The selected combinations focused on the borderline shown in Fig. 8. Fig. 9 shows a comparison of cell performance for these four different H_2/O_2 inlet mole fraction combinations. The figure shows that increasing the hydrogen inlet mole fraction and decreasing the oxygen inlet mole fraction leads to better cell performance. However, this trend should be controlled so as not to lead to a negative value of oxygen molar fraction within the cell and failure of the solution procedure. As shown, the H_2/O_2 inlet mole fraction of 0.96/0.02 showed the best performance among all the safe combinations of H_2/O_2 inlet mole fractions in this study, with the same other inputs. This cell produces about 2180W/m^2 maximum power density. However, the value for AP-SOFC in unsafe conditions (as shown in Fig. 2) was 2540 W/m^2. Considering the safety issue by controlling the H_2/O_2 inlet mole fraction thus reduces the cell performance by 14%.

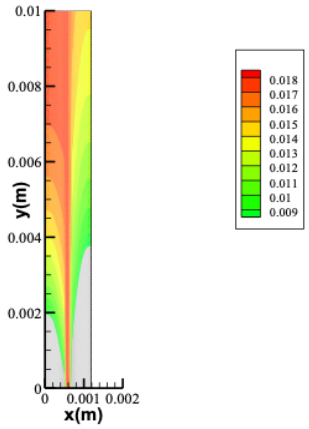

Case1: $x_{H_2} = 0.7$ $x_{O_2} = 0.1$

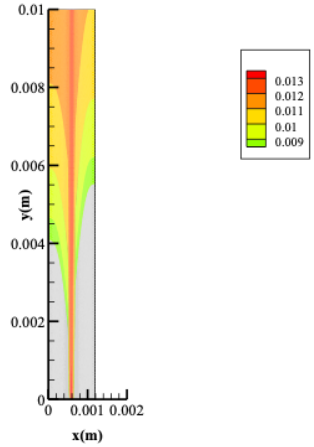

Case2: $x_{H_2} = 0.5$ $x_{O_2} = 0.1$

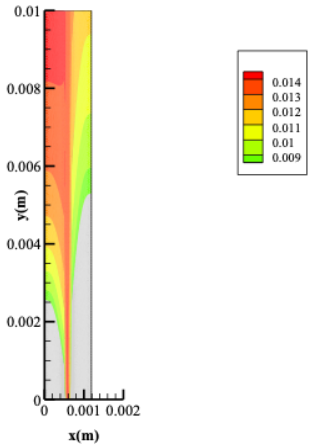

Case3: $x_{H_2} = 0.7$ $x_{O_2} = 0.08$

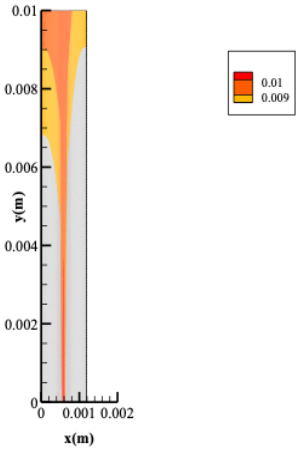

Case4: $x_{H_2} = 0.5$ $x_{O_2} = 0.08$

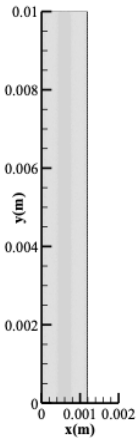

Case5: $x_{H_2} = 0.83$ $x_{O_2} = 0.03$

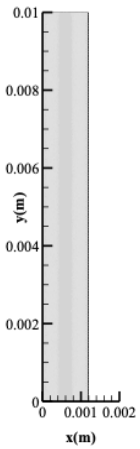

Case6: $x_{H_2} = 0.96$ $x_{O_2} = 0.02$

Fig. 7. H_2×O_2 mole fraction product at cell voltage 0.7 V in 30% electrolyte porosity AP-SOFC for different combinations of the H_2 and O_2 inlet mole fraction.

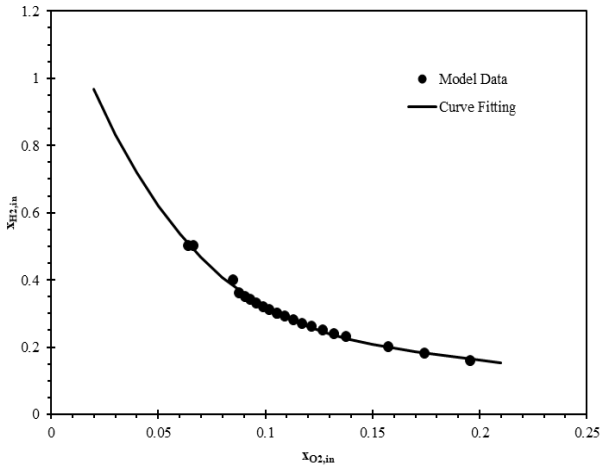

Fig. 8. Presentation of H2/O2 inlet mole fraction combinations guaranteeing safe operation at cell voltage 0.7 V.

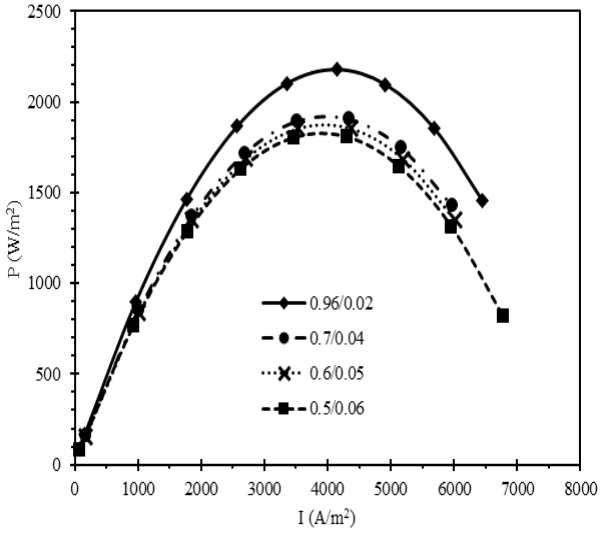

Fig. 9. Comparison of the cell performance with different H_2/O_2 inlet mole fraction combinations under safe conditions.

5. Conclusion

The numerical investigation of a hydrogen fuelled planar all-porous solid oxide fuel cell to analyze safe operation regions has been reported. A comparative performance study between conventional and all-porous solid oxide fuel cell schemes showed that oxygen transport from the cathode to the anode, on one hand, and hydrogen and water from the anode to the cathode, on the other side, led to a reduction in cell performance in the porous electrolyte scheme. Furthermore, considering the Lower Explosive Limit of hydrogen in the air reveals that all the all-porous schemes were not safe compared to a conventional scheme with the same fuel input. Different combinations in H_2 and O_2 inlet mole fractions were simulated in order to achieve fully safe operations, as well as an improved cell performance. Finally, the all-porous solid oxide fuel cell with was revealed to be the best performance in safe operating conditions.

References

[1] Pittock A.B., 2nd ed., Climate change the science, impacts and solutions, CSIRO, 2009.

[2] EG and G Technical Services, Inc. Science Applications International Corporation, 6th ed., Fuel Cell Handbook, US Department of Energy,2002 .

[3] Ghassemi M., Kamvar M. and Steinberger-wilckens R., 1st ed., Fundamentals of heat and fluid flow in high temperature fuel cells, Elsevier, 2020.

[4] Bove R. and Ubertini S., 1th ed., Modeling Solid Oxide Fuel Cells, Methods, Procedures and Technologies, Springer, 2008.

[5] Kupecki J., Papurello D., Lanzini A., Naumovich Y., Motylinski K., Blesznowski M and Santarelli M., "Numerical model of planar anode supported solid oxide fuel cell fed with fuel containing H_2S operating in direct internal reforming mode (DIR-SOFC)", J. Applied Energy, 2018, 230: 1573.

[6] Kim S., Jang I., Kim Ch., Lee H., Song T., Yoon H. and Paik U., "Enhanced reliability of planar-type solid oxide fuel cell stack incorporating leakage gas induction channels", Int. J. Hydrogen Energy, 2020, 45: 11834.

[7] Hibino T. and Iwahara H., "Simplification of solid oxide fuel cell system using partial oxidation of methane", Chemistry Letters, 1993, 22: 1131.

[8] Tian Y., Wu P., Zhang X., Guo X. and Ding L., "Performance of a linear array solid oxide fuel cell micro-stack operated in single-chamber conditions" J. Ionics, 2020, 26: 6217.

[9] Kamvar M., Ghassemi M. and Rezaei M., "Effect of catalyst layer configuration on single chamber solid oxide fuel cell performance", J. Applied Thermal Engineering, 2016, 100: 98.

[10] Kamvar M., Ghassemi M. and Steinberger-Wilckens R., "The numerical investigation of a planar single chamber solid oxide fuel cell performance with a focus on the support types", Int. J. Hydrogen Energy, 2020, 45: 7077.

[11] Tian Y., Lu Zh., Wang Zh., Wei B., Nie Zh. And Zhai A., "Enhanced performance of a single-chamber solid oxide fuel cell with dual gas supply method", Ionics, 2019, 25: 1281.

[12] Bedon A., Viricelle J.P., Rieu M., Mascotto S. and Glisenti A., "Single chamber solid oxide ful cells selective electrodes: A real chance with brownmillerite-based nanocomposites" Int. J. Hydrogen Energy, 2021, 46:14735.

[13] Akhtar N., Decent S. P., Loghin D. and Kendall K., "A three dimensional numerical model of a single-chamber solid oxide fuel cell", Int. J. Hydrogen Energy, 2009, 34: 8645.

[14] Akhtar N., Decent S. P., Loghin D. and Kendall K., "Mixed-reactant, micro-tubular solid oxide fuels: An experimental study", J. Power Sources, 2009, 193: 39.

[15] Akhtar N. and Kendall K., "Micro-tubular, solid oxide fuel cell stack operated under single-chamber conditions", Int. J. Hydrogen Energy, 2011, 36: 13083.

[16] Akhtar N., Decent S. P. and Kendall K., "Numerical modelling of methane-powered micro-tubular, single-chamber solid oxide fuel cell", J. Power Sources, 2010, 195: 7796.

[17] Akhtar N., Decent S. P. and Kendall K., "A parametric analysis of a micro-tubular, single-chamber solid oxide fuel cell (MT-SC-SOFC)", Int. J. Hydrogen Energy, 2011, 36: 765.

[18] Akhtar N., "Micro-tubular, single-chamber solid oxide fuel cell (MT-SC-SOFC) stacks: Model development", Chemical Engineering Research and Design, 2012, 90: 814.

[19] Akhtar N., "Modeling of novel porous inserted micro-tubular, single-chamber solid oxide fuel cells (MT-SC-SOFC)", Chemical Engineering Journal, 2012, 179: 277.

[20] Kamvar M. and Ghassemi M., "Performance analysis of coplanar single chamber solid oxide fuel cell with oxygen-methane-nitrogen mixture under steady state conditions", J. Modares Mechanical Engineering, 2017, 17: 31

[21] Guo Y.M., Bessaa M., Aquado S., Cesar Steil M., Rembelski D., Rieu M., et al., "An all porous solid ocide fuel cell (SOFC): a bridging technology between dual and single chamber SOFCs", Energy Environ. Sci., 2013, 6: 2119.

[22] Guo Y.M., Largiller G., Guizard C., Tardivat C. and Farrusseng D., "Coke-free operation of an all porous solid oxide fuel cell (AP-SOFC) used as an O_2 supply device", J Materials Chemistry A, 2015, 3: 2684.

[23] Xu H., Chen B., Tan P., Cai W., He W., et al., "Modelling of all porous solid oxide fuel cells", Applied Energy, 2018, 219: 105.

[24] Xu H., Chen B., Tan P., Xuan J., Mercedes M., et al., "Modelling of all-porous solid oxide fuel cells with a focus on the electrolyte porosity design", Applied Energy, 2019, 235: 602.

[25] Xu H., Chen B., Tan P., Zhang Y., He Q., et al., "The thermal effects of all-porous solid oxide fuel cells", J. Power Sources, 2019, 440: 227102.

[26] Kamlungsua K., Su P. C. and Chan S. H., "Hydrogen generation using solid oxide electrolysis cells", Fuel cells, 2020, 6: 644.

[27] M. Kamvar, "Comparative numerical study of co- and counter-flow configurations of an all-porous solid oxide fuel cell", Iranian J of Hydrogen & Fuel Cell, 2021, 2: 77.

[28] Timurkutluk B., Celik S., Timurkutluk C., Mat M.D. and Kaplan Y., "Novel electrolytes for solid oxide fuel cells with improved mechanical properties", Int. J. Hydrogen Energy, 2012, 37: 13499.

[29] Nield D.A. and Bejan A., 3rd ed., Convection in Porous Media, Springer, 2006.

[30] Batchelor G.K., 1st ed., An Introduction To Fluid Dynamics, Cambridge University Press, 2000.

[31] Taylor R. and Krishna R., 1th ed., Multicomponent mass transfer, John Willey & Sons, Inc., 1993.

[32] Cengel Y.A. and Ghajar A. J., 5th ed., Heat and mass transfer fundamentals & applications, MC Graw Hill, 2014.